Time-Extracting Wavelet Transform for Characterizing Impulsive-Like Signals and Theoretical Analysis

Wenting Li, Zhuosheng Zhang, François Auger, Xiangxiang Zhu

Noname manuscript No.
(will be inserted by the editor)

Time-extracting wavelet transform for characterizing impulsive-like signals and theoretical analysis

Wenting Li[1] · **Zhuosheng Zhang**[1] · **François Auger**[2] · **Xiangxiang Zhu**[3]

Received: date / Accepted: date

Abstract In this paper, a high-resolution time-frequency (TF) analysis method, called time-extracting wavelet transform (TEWT) is introduced to analyze impulsive-like signals whose TF ridge curves are nearly perpendicular to the time axis. For impulsive-like signals, the instantaneous frequency with almost infinite rate of change is difficult to estimate, but the group delay (GD) with nearly zero rate of change is easier to estimate. Since the GD is the key feature of frequency-domain signals, it indicates that one can try to understand impulsive-like signals from the perspective of frequency-domain signals. In this regard, for an impulsive signal and its Fourier transform (i.e. the frequency-domain harmonic signal), we propose the TEWT that achieves highly-concentrated TF representations while allowing signal reconstruction, only by retaining the TF energy closely related to TF features of signals, while removing

Wenting Li
E-mail: wenting1990@stu.xjtu.edu.cn
Zhuosheng Zhang
E-mail: zszhang@mail.xjtu.edu.cn
François Auger
E-mail: francois.auger@univ-nantes.fr
Xiangxiang Zhu
E-mail: zhuxiangxiang@nwpu.edu.cn
[1] School of Mathematics and Statistics, Xi'an Jiaotong University, Xi'an 710049, China
[2] Nantes Université, Institut de Recherche en Énergie Électrique de Nantes Atlantique (IREENA, UR 4642), Saint-Nazaire, France
[3] School of Mathematics and Statistics, Northwestern Polytechnical University, Xi'an 710049, China

weakly-related TF information. The two contributions of this paper are the proposal of TEWT and the theoretical analysis of TEWT for frequency-domain signals. On the other hand, we provide a rigorous theoretical analysis of TEWT under a mathematical framework for frequency-domain signals. Specifically, we define a function class as a set of all superposition of well-separated frequency-domain harmonic-like functions, where each function can be locally regarded as a sum of a finite number of harmonic signals in the frequency domain, and establish error bounds for WT approximate expression, GD estimation and component recovery. Finally, we verify the effectiveness of TEWT in terms of the energy concentration, robustness, and invertibility through numerical experiments with synthetic and real signals.

Keywords Time-frequency analysis · Synchrosqueezing · Time-extracting wavelet transform · Group delay · Signal reconstruction

1 Introduction

Multi-component non-stationary signals are ubiquitous in the physical world, widely appearing in mechanical engineering [28, 30], animal sounds [27], seismic signals [25], etc. Time-frequency (TF) analysis (TFA) methods provide a powerful tool for characterizing multi-component non-stationary signals. Traditional TFA methods can be roughly divided into linear TFAs [26] and quadratic TFAs [7], but they are limited by their inherent properties. Linear TFAs, such as short-time Fourier transform (STFT) and wavelet transform (WT), localize the TF feature by calculating the inner product between the signal and the basis function, but TF concentration is subject to Heisenberg uncertainty principle; quadratic TFAs, such as the Wigner-Ville distribution and its variants, achieve perfect TF resolution by calculating the Fourier transform (FT) of the local signal correlation, but introduce unexpected cross-terms for multi-component signals. In order to overcome these shortcomings, some effective TF post-processing techniques such as reassignment methods (RM) [1, 18, 19], synchrosqueezing methods [8, 9] and synchroextracting methods [39] have been proposed in recent years.

The RM was first introduced by Kodera et al. to the spectrogram [18, 19], and generalized by Auger and Flandrin to any bilinear TF or time-scale distribution [1]. The RM method reassigns the TF coefficients from the original position to the centroid of energy distribution of the signal, both along the time axis and the frequency axis, so as to obtain a more concentrated TFR in the TF plane [6, 10], but it cannot reconstruct the signal. As a special case of RM [2], Daubechies and Maes proposed synchrosqueezing wavelet transform (SWT) that squeezes the WT coefficients along the frequency direction with the capability of sharpening and reversible TFRs [8], as an empirical mode decomposition (EMD) tool [16]. Subsequently, SWT was extended to other TF transforms, such as STFT [32] and S-transform [17].

Generally speaking, a multi-component non-stationary signal is modeled as:

$$x(t) = \sum_{k=1}^{K} x_k(t) = \sum_{k=1}^{K} a_k(t) e^{i\varphi_k(t)}, \tag{1}$$

where $a_k(t)$ and $\varphi_k(t)$ are respectively the instantaneous amplitude and instantaneous phase of the kth component $x_k(t)$ of $x(t)$, the derivative of $\varphi_k(t)$ is the instantaneous frequency (IF) $\varphi_k'(t)$ and its second-order derivative is the chirp rate $\varphi_k''(t)$. When the component $x_k(t)$ satisfies $|a_k'(t)|, |\varphi_k''(t)| \le \epsilon |\varphi_k'(t)|$ ($\epsilon > 0$ is sufficiently small), which can be locally regarded as a harmonic signal showing horizontal lines in the TFR [8], SWT can reach highly concentrated TFRs and exact invertible properties. Also suitable for describing slowly varying signals is the recently proposed SET that achieves a high-resolution TFR [39], only by retaining the closely-related TF coefficients while discarding weakly-related TF coefficients. However, SWT and SET suffer from blurred TFRs for signals with fast varying IF. Thus some extensions of SWT have been developed, such as the second-order cases [5, 35], high-order cases [15, 29], demodulation cases [20, 31, 33, 34], and multiple squeezes transform [37, 38, 42]. Besides, there are also some extensions about SET [13, 21, 23, 40, 41].

Among these extensions, Wang et al. proposed a matching synchrosqueezing wavelet transform (MSWT) designed for fast varying signals satisfying $|\varphi_k''(t)| < \infty$ [35]. It can be found that SWT, SET and their improved methods are mostly suitable for characterizing slowly varying signals (such as $|\varphi_k''(t)| \to 0$ in SWT) and strongly varying signals (such as $|\varphi_k''(t)| < \infty$ in MSWT), but not suitable for characterizing impulsive-like signals whose TF ridge curves are nearly parallel with frequency axis, where ridge curves are the curves at the TF plane along which the signal energy is locally maximum [24]. In order to overcome the limitation, some recently proposed TFA techniques, called time-reassigned synchrosqueezing transform (TSST) [14], time-reassigned synchrosqueezing wavelet transform (TSWT) [22], and transient-extracting transform [36] can effectively characterize impulsive-like signals satisfying $|\varphi_k''(t)| \to \infty$. TSST is the time squeezing method under the STFT framework, we generalize TSST to the WT framework, propose TSWT and provide a theoretical analysis of TSWT [14]. In this paper, we further extend TET to the WT framework to introduce a new post-processing TFA method.

The two contributions of this paper are the proposal of time-extracting wavelet transform (TEWT) and the theoretical analysis of TEWT for frequency domain signals. In this paper, for impulsive signals and its frequency-domain harmonic signals, we introduce the TEWT, only by retaining the TF energy closely related to the TF features of the signal while removing weakly-related TF information, which not only achieves highly concentrated TFRs, but also considers signal reconstruction. Most importantly, we provide the theoretical analysis of TEWT under a strict mathematical framework for the frequency-domain signal model. The remainder of this paper is organized as follows. In Section 2, WT, SWT and TSST are reviewed. In Section 3, we introduce a TEWT designed for impulsive signals and its frequency-domain harmonic signals. Section 4 is devoted to study the theoretical analysis of the TEWT, we define a function class as a set of all superposition of well-separated frequency-domain harmonic-like functions, where each function can be locally regarded as a sum of a finite number of harmonic signals in the frequency domain, and establish error bounds for WT approximate expression, GD estimation and component recovery for this class. Section 5 verifies the TF concentration, robustness, and invertibility of the TEWT by using numerical experiments of frequency-domain signals, time-domain signals and real signals with two quantitative indicators. Finally, conclusions are drawn in Section 6.

2 Synchrosqueezing wavelet transform and Time-reassigned synchrosqueezing transform

2.1 Synchrosqueezing wavelet transform (SWT)

The Fourier transform (FT) of a signal $x(t)$ is defined by [26]:

$$X(\omega) = \int_R x(t)e^{-i\omega t}dt, \tag{2}$$

and its inverse FT is defined by [26]:

$$x(t) = \frac{1}{2\pi}\int_R X(\omega)e^{i\omega t}d\omega. \tag{3}$$

The WT of a signal $x(t)$ with an admissible wavelet $\psi(t)$ is defined by [26]

$$W_x^{\psi}(b,a) = \frac{1}{a}\int_R x(t)\psi^*(\frac{t-b}{a})dt. \tag{4}$$

where ψ^* is the complex conjugate of ψ. By Plancherel's theorem, the WT $W_x^{\psi}(b,a)$ can be rewritten as [26]

$$W_X^{\hat{\psi}}(b,a) = \frac{1}{2\pi}\int_R X(\omega)\hat{\psi}^*(a\omega)e^{i\omega b}d\omega. \tag{5}$$

where the $\hat{\psi}$ is the FT of ψ. It has been proven that in [8] ,

$$\begin{aligned}\int_{R^+} W_x^{\psi}(b,a)\frac{da}{a} &= \frac{1}{2\pi}\int_{R^+}(\int_R \hat{\psi}^*(a\omega)\frac{da}{a})X(\omega)e^{i\omega b}d\omega \\ &= (\int_{R^+}\hat{\psi}^*(\eta)\frac{d\eta}{\eta})(\frac{1}{2\pi}\int_R X(\omega)e^{i\omega b}d\omega) \\ &= x(b)C_{\psi},\end{aligned} \tag{6}$$

setting $C_{\psi} = \int_{R^+}\hat{\psi}^*(\eta)\frac{d\eta}{\eta}$, then the signal can be reconstructed by WT,

$$x(b) = \frac{1}{C_{\psi}}\int_{R^+} W_x^{\psi}(b,a)\frac{da}{a}. \tag{7}$$

The complex reassignment operators $\tilde{t}_x(b,a)$ and $\tilde{\omega}_x(b,a)$ can be defined wherever $W_x^{\psi}(b,a) \neq 0$ by [10]

$$\begin{cases}\tilde{t}_x(b,a) = b + a\frac{W_x^{t\psi}(b,a)}{W_x^{\psi}(b,a)} \\ \tilde{\omega}_x(b,a) = -i\frac{\partial_b W_x^{\psi}(b,a)}{W_x^{\psi}(b,a)}\end{cases} \tag{8}$$

where ∂_b is the partial derivative with respect to b, and $\hat{t}_x(b,a) = \Re\{\tilde{t}_x(b,a)\}$ is the real part of complex time reassignment operator.

The SWT proposed by Daubechies et al. [8] provides an alternative theoretical way to understand the principle of EMD [16], which is performed via three successive steps. The first step is to calculate the WT expression $W_x^{\psi}(b,a)$ of the analyzed signal $x(t)$ (1) by (4). The second step is to calculate a candidate IF $\tilde{\omega}_x(b,a)$ for $x(t)$ by (8). The final step is to reallocate the TF energy from the (b,a) plane to the $(b,\tilde{\omega}_x(b,a))$ plane in the frequency direction:

$$T_x(b,\omega) = \int_{A_{x,\epsilon}(b)} W_x^{\psi}(b,a)a^{-\frac{3}{2}}\delta(\omega - \tilde{\omega}_x(b,a))da. \tag{9}$$

where $A_{x,\epsilon}(b) := \{a \in R^+; |W_x^{\psi}(b,a)| > \epsilon\}$. Studies show that the SWT $T_x(b,\omega)$ can obtain reasonable accuracy while dealing with harmonic-like signals (i.e. $|a_k'(t)|, |\varphi_k''(t)| \leq \epsilon|\varphi_k'(t)|$) [2, 8] in the time domain, whose TF ridge curves are almost parallel to the time axis.

2.2 Time-reassigned synchrosqueezing transform (TSST)

Under the WT framework, SWT uses the IF estimator to reassign the TF energy in the frequency direction, while the TSST under the STFT framework uses the GD estimator to reassign the TF energy in the time direction [14]. The TSST is also performed via three successive steps. The first step is to calculate the STFT representation $S_x^h(b,\omega)$ of $x(t)$ with a window function $h(t)$,

$$S_x^h(b,\omega) = \int_R x(t)h(t-b)e^{-i\omega t}dt. \tag{10}$$

The second step is to calculate a candidate GD for $x(t)$ ($S_x^h(b,\omega) \neq 0$):

$$\hat{t}_x(b,\omega) = -\Im\{\frac{\partial_\omega S_x^h(b,\omega)}{S_x^h(b,\omega)}\}. \tag{11}$$

where $\Im\{z\}$ is the imaginary part of z. The final step is energy reallocation,

$$V_x(t,\omega) = \int_{B_{x,\epsilon}(b)} S_x^h(b,\omega)\delta(t - \hat{t}_x(b,\omega))db. \tag{12}$$

where $B_{x,\epsilon}(b) := \{\omega \in R; |S_x^h(b,\omega)| > \epsilon\}$. As a post-processing method of STFT, TSST reassigns the TF information from each point (b,ω) to $(\hat{t}_x(b,\omega),\omega)$ along the time direction. By calculating an exact GD estimator $\hat{t}_x(b,\omega)$ of impulsive signal, TSST can squeezes diffused STFT coefficients near $(\hat{t}_x(b,\omega),\omega)$ to obtain a concentrated TFR. Study shows that the TSST improves the energy concentration of the

TFR for impulsive-like signals (i.e. $|\varphi_k''(t)| \to \infty$) [14], whose TF ridge curves are almost perpendicular to the time axis. However, TSST is designed for time-domain impulsive-like signals, and does not consider frequency-domain signal models. For further theoretical analysis, we propose a new TFA to analyze impulsive-like signals or even frequency-domain signals in the next section.

3 Time-extracting wavelet transform (TEWT)

In this section, we propose a new post-processing tool of WT, named time-extracting wavelet transform (TEWT), to improve the energy concentration of the TFRs for impulsive signals or frequency-domain harmonic signals, whose TF ridge curves are almost perpendicular to the time axis.

3.1 TEWT designed for impulsive signal

To motivate the idea, an impulsive signal $x(t)$ that has the perfect time location property is considered [14],

$$x(t) = A\delta(t - t_0), \tag{13}$$

where the Dirac function $\delta(t)$ is the ideal model for describing the impulsive signal $x(t)$ only appearing at one time instant t_0. Substituting Eq. (13) into Eq. (4) leads to WT of $x(t)$,

$$\begin{aligned} W_x^{\psi}(b,a) &= \frac{1}{a}\int_R A\delta(t-t_0)\psi^*(\frac{t-b}{a})dt \\ &= \frac{1}{a}A\psi^*(\frac{t_0-b}{a}). \end{aligned} \tag{14}$$

According to (14), if $\psi(t)$ is concentrated around $t = 0$, then $W_x^{\psi}(b,a)$ will be spread around the line $b = t_0$ and suffer from a blurred TFR. Meanwhile, the local maximum point of the WT modulus $|W_x^{\psi}(b,a)|$, that is, the ridge point [24], is exactly on the GD curve $b = t_0$ of the signal, where the GD may be estimated by a GD candidate $\hat{t}_x(b,a)$ [10]. Then by (8), the WT $W_x^{t\psi}(b,a)$ of $x(t)$ with respect to $t\psi(t)$ can be expressed as

$$\begin{aligned} W_x^{t\psi}(b,a) &= \frac{1}{a}\int_R A\delta(t-t_0)(\frac{t-b}{a})\psi^*(\frac{t-b}{a})dt \\ &= \frac{1}{a}A(\frac{t_0-b}{a})\psi^*(\frac{t_0-b}{a}), \end{aligned} \tag{15}$$

According to Eqs. (8), (14) and (15), $\hat{t}_x(b,a)$ can be calculated as

$$\hat{t}_x(b,a) = t_0. \tag{16}$$

It is clear that the time reassignment operator $\hat{t}_x(b,a)$ can be an exact GD estimator of the impulsive signal $x(t)$, and the WT modulus also reaches its maximum value at $b = \hat{t}_x(b,a)$.

Therefore, in order to achieve a more concentrated TFR, we introduce the TEWT only by retaining the WT coefficients on the ridge point $b = \hat{t}_x(b,a)$,

$$Te(b,a) = W_x^{\psi}(b,a) \cdot \delta(b - \hat{t}_x(b,a)). \tag{17}$$

Combing Eqs. (14), (16) and (17), we can further derive the TEWT result of impulsive signal,

$$Te(b,a) = \frac{1}{a}\psi^*(0) \cdot A\delta(b - t_0). \tag{18}$$

In order to compare the energy concentration of the WT and the TEWT more intuitively, we employ a discrete impulsive signal, being sampled at 256 Hz and $A = 1$, $t_0 = 0.5$, where its waveform and frequency spectrum are shown in Fig. 1 (a), (b). It shows that the impulsive signal has the best time location and the worst frequency location. Fig. 1 (c) and (d) show the WT result and its slice at $\omega_0 = 64$ Hz, it can be observed that WT obtains a blurred TFR and its energy distribution spreads around the time $b = t_0$. Furthermore, Fig. 1 (e) and (f) show the TEWT result and its slice at $\omega_0 = 64$ Hz, it can be seen that the energy distribution of the TEWT is highly concentrated and only appears at time $b = t_0$, which demonstrates that TEWT can improve energy concentration of blurred WT result for the impulsive signal.

Furthermore, we employ the Rényi entropy [3, 4] to evaluate the energy concentration of the TEWT quantitatively, which is defined as

$$R^{\alpha} = \frac{1}{1-\alpha}\log_2 \int\int (\frac{TFR(t,\omega)}{\int\int TFR(t,\omega)dtd\omega})^{\alpha} dtd\omega. \tag{19}$$

Generally, a lower Rényi entropy value indicates a more energy-concentrated TFR. The following table 1 lists third-order Rényi entropies of WT and TEWT under four signal-to-noise ratios (SNRs), where impulsive signal is added with Gaussian white noises. It shows that, the TEWT obtains the lower Rényi entropies than WT under

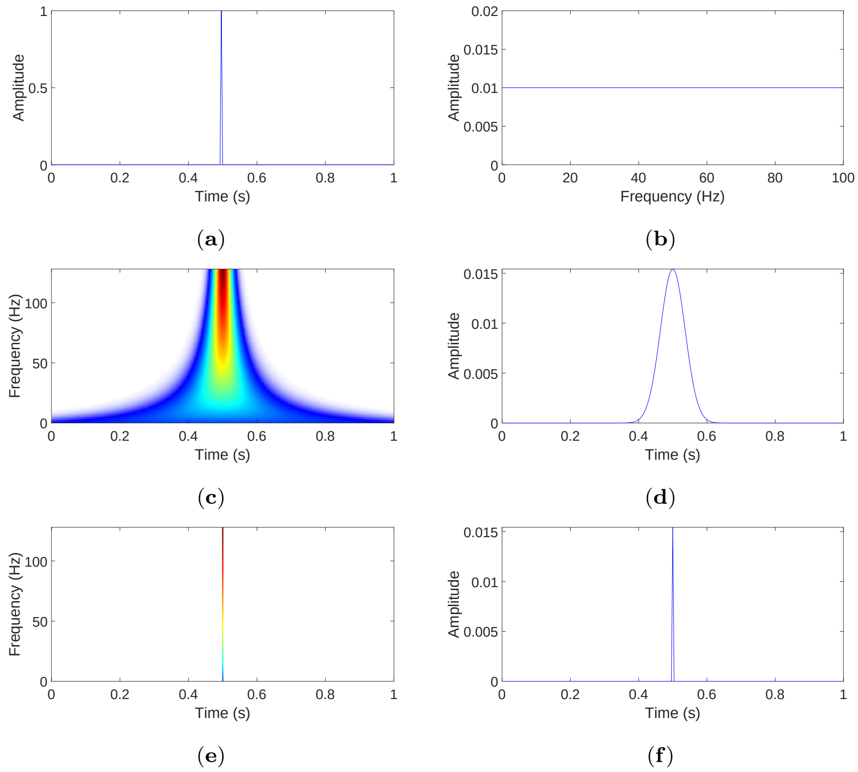

Fig. 1: (a) Time-domain impulsive signal with $t_0 = 0.5$ s. (b) Frequency-domain harmonic signal. (c) WT result. (d) Slice of the WT modulus at $\omega_0 = 64$ Hz, i.e., $|W_x^{\psi}(b, \omega_0)|$. (e) TEWT result. (f) Slice of the TEWT modulus at $\omega_0 = 64$ Hz, i.e., $|Te(b, \omega_0)|$.

Table 1: Rényi entropies obtained by WT and TEWT under different SNRs.

	SNR=-5dB	SNR=0dB	SNR=5dB	SNR=10dB
WT	6.3265	5.9838	5.5351	5.1177
TEWT	2.6757	2.1394	1.3191	0.5303

four noise levels , which means that TEWT can generate a more energy-concentrated TFR than WT.

Finally, TEWT maintains the reconstructed property of WT by (7),

$$x(b) = \frac{1}{C_\psi} \int_{R^+} Te(b, a) \frac{da}{a}. \tag{20}$$

Compared with TSST, which is also designed for impulsive signals, TEWT extracts the WT coefficients at the $b = \hat{t}_x(b, a)$ instead of reassigning the STFT coefficients in TSST. In other words, TSST reassigns the STFT coefficients from the (b, ω) plane to the $(\hat{t}_x(b,\omega),\omega)$ plane along the time direction, while TEWT retains the WT coefficients on the $b=\hat{t}_x(b,a)$ that is closely related to the TF features of the signal, so as to achieve a high-resolution TFR. It can be concluded that TEWT provides a new tool for characterizing and recovering impulsive signals.

3.2 TEWT designed for frequency-domain harmonic signal

The key step of the TEWT is the GD estimation, and the GD is the crucial feature of a frequency-domain signal, it follows that one can try to understand impulsive signals from the perspective of frequency-domain signal, and frequency-domain signal can be defined by

$$X(\omega)=A(\omega)e^{-i\phi(\omega)}. \tag{21}$$

where $A(\omega)$ is the signal amplitude, $\phi(\omega)$ and its derivative $\phi'(\omega)$ are the phase and the GD of the frequency-domain signal $X(\omega)$, respectively.

Back to the time-domain impulsive signal $x(t)=A\delta(t-t_0)$ (13) in the previous subsection, the change-rate of IF is nearly infinite, which means that its IF is difficult to be approximated. Through FT (2), its frequency domain form can be written as

$$\begin{aligned} X(\omega)&=\int_R A\delta(t-t_0)e^{-i\omega t}dt \\ &=Ae^{-i\omega t_0}. \end{aligned} \tag{22}$$

Contrast with (21), we have $A(\omega)=A$, $\phi(\omega)=\omega t_0$, the GD $\phi'(\omega)=t_0$ and its change-rate $\phi''(\omega)=0$, which indicates the GD is easier to be estimated than the IF. It follows that an impulsive signal $x(t)$ with strongly-varying IF in the time domain becomes a harmonic signal $X(\omega)$ with slowly-varying GD in the frequency domain. In other words, for impulsive-like signals, time-domain signals with high-order IF approximation can be replaced by frequency-domain signals with low-order GD approximation. Therefore, it is necessary to perform TEWT analysis on frequency domain signals.

Similar to impulsive signals in the time domain, TEWT based on frequency-domain harmonic signals is also performed via three successive steps, starting with calculating WT. And the WTs of $X(\omega)$ with respect to $\hat{\psi}(\omega)$ and $\hat{\psi}'(\omega)$ are respectively

$$\begin{aligned} W_X^{\hat{\psi}}(b,a) &= \frac{1}{2\pi}\int_R Ae^{-i\omega(b-t_0)}\hat{\psi}^*(a\omega)d\omega \\ &= \frac{1}{a}A\psi^*(\frac{t_0-b}{a}), \end{aligned} \tag{23}$$

$$\begin{aligned} W_X^{\hat{\psi}'}(b,a) &= \frac{1}{2\pi}\int_R Ae^{-i\omega(b-t_0)}\hat{\psi}'^*(a\omega)d\omega \\ &= \frac{i}{a}A(\frac{t_0-b}{a})\psi^*(\frac{t_0-b}{a}). \end{aligned} \tag{24}$$

It can be seen that the WT result given by Eq. (23) is consistent with Eq. (14). The second step is to calculate a candidate GD $\hat{t}_X(b,a)$. Substituting Eqs. (23), (24) into Eq. (8) leads to the same expression as Eq. (16),

$$\hat{t}_X(b,a) = b + a\Im\{\frac{W_X^{\hat{\psi}'}(b,a)}{W_X^{\hat{\psi}}(b,a)}\} = t_0. \tag{25}$$

where $(-it)\psi(t) \xrightarrow{F} \hat{\psi}'(\omega)$. It also demonstrates that $\hat{t}_X(b,a)$ provides an exact GD estimation for frequency-domain harmonic signal, then $\hat{t}_X(b,a)$ is called a first-order GD estimator. The final step is to obtain the same TEWT result as (18) by retaining the TF information at $b = \hat{t}_X(b,a)$,

$$\begin{aligned} Te(b,a) &= W_X^{\hat{\psi}}(b,a)\cdot\delta(b-\hat{t}_X(b,a)) \\ &= \frac{1}{a}\psi^*(0)\cdot A\delta(b-t_0). \end{aligned} \tag{26}$$

In a discrete situation, we consider the TEWT $Te(b,a)$ in the TF plane instead of the time-scale plane, which is implemented by the following expression

$$Te(n,m) = \begin{cases} W_x^{\psi}(n,m), & if\ |n-\phi'(m)| < \frac{\Delta n}{2} \\ 0, & otherwise \end{cases} \tag{27}$$

where n, m and Δn denote the discrete time variable, frequency variable and the sampling time interval respectively. By Eq. (27), it shows that TEWT retains the TF energy of the WT result in the TF region $n \in (\phi'(m)-\frac{\Delta n}{2},\ \phi'(m)+\frac{\Delta n}{2})$, while TEWT removes the TF energy in the TF region $n \notin (\phi'(m)-\frac{\Delta n}{2},\ \phi'(m)+\frac{\Delta n}{2})$. It follows that the TEWT only retains the closely-related TF energy while discarding weakly-related TF coefficients. Therefore, TEWT can achieve a highly resolution TFR for frequency-domain harmonic signals.

Finally, the TEWT reconstruction formula we designed for frequency domain harmonic signals is different from (20), but it still needs to start from WT reconstruction, which requires evaluating the WT in (23) along the ridge line $b = t_0$ leads to

$$W_X^{\hat{\psi}}(t_0, a) = \frac{1}{a} A\psi^*(0). \tag{28}$$

Then, the frequency-domain harmonic signal can be obtained by

$$X(\frac{\omega_\psi}{a}) = \frac{aW_X^{\hat{\psi}}(t_0, a)e^{-i\frac{\omega_\psi}{a}t_0}}{\psi^*(0)}, \tag{29}$$

where ω_ψ is the center frequency of $\hat{\psi}(\omega)$. It motivates us to recover the signal from the TEWT result with a similar reconstruction expression as follows:

$$X(\frac{\omega_\psi}{a}) = \frac{aTe(t_0, a)e^{-i\frac{\omega_\psi}{a}t_0}}{\psi^*(0)}, \tag{30}$$

which means that TEWT also maintains the invertible property for frequency-domain harmonic signals.

Compared with SWT and TSST, the frequency-domain harmonic signal in the TEWT replaces the time-domain harmonic signal in the SWT, the GD estimator of TEWT replaces the IF estimator of SWT, the extracting manner of TEWT replaces the synchrosqueezing way of SWT and TSST, thus TEWT is a different post-processing method from SWT and TSST. It can also be concluded that TEWT provides a powerful tool for the analysis and reconstruction of time-domain impulsive signals or frequency-domain harmonic signals.

4 Theoretical analysis of TEWT

In this section, we provide a mathematically rigorous theorem of TEWT that can identify and characterize a class of functions $\mathcal{H}_{\epsilon,d}$ in the frequency domain, containing harmonic-like functions that are well separated, which is different from the class $\mathcal{A}_{\epsilon,d}$ of SWT [8]. We start with the following definition.

Definition 1 The class $\mathcal{H}_{\epsilon,d}$ is said to be a set of all superposition of well-separated frequency-domain harmonic-like functions (FHF) up to accuracy $\epsilon > 0$ and with separation $d > 0$, if each element $X(\omega) = \sum_{k=1}^{K} X_k(\omega) = \sum_{k=1}^{K} A_k(\omega)e^{-i\phi_k(\omega)} \in \mathcal{H}_{\epsilon,d}$ satisfies the following two properties:

(1) For $k \in \{1, 2, ..., K\}$, functions $X_k(\omega)$ with $A_k(\omega)$ and $\phi_k(\omega)$ satisfy:

$$
\begin{aligned}
&A_k(\omega) \in C^1(R) \cap L^\infty(R), \quad \phi_k(\omega) \in C^2(R), \\
&0 < m_k = \inf_{\omega \in R^+} A_k(\omega) \le \sup_{\omega \in R^+} A_k(\omega) = M_k < \infty, \\
&0 < \inf_{\omega \in R^+} \phi_k'(\omega) \le \sup_{\omega \in R^+} \phi_k'(\omega) = M_k' < \infty, \\
&|A_k'(\omega)|, \ |\phi_k''(\omega)| \le \epsilon |\phi_k'(\omega)|, \ \forall \omega \in R^+.
\end{aligned}
\tag{31}
$$

(2) For $k \in \{1, 2, ..., K-1\}$, functions $X_k(\omega)$ are well separated with d, i.e.

$$
\phi_{k+1}'(\omega) - \phi_k'(\omega) \ge \frac{d}{\omega}, \quad \forall \omega \in R^+. \tag{32}
$$

Remark. Compared with the class $\mathcal{A}_{\epsilon,d}$ of SWT [8], each function $X(\omega) \in \mathcal{H}_{\epsilon,d}$ is composed of several frequency-domain components $X_k(\omega)$ with slowly frequency-varying amplitude $A_k(\omega)$ and GD $\phi_k'(\omega)$, thus the component $X_k(\omega)$ can be locally regarded as a harmonic signal with small change-rate of amplitude $A_k(\omega)$ and GD $\phi_k'(\omega)$ in the frequency domain. While each function $x(t) = \sum_{k=1}^{K} x_k(t) \in \mathcal{A}_{\epsilon,d}$ is composed of several time-domain components $x_k(t) = a_k(t)e^{i\varphi_k(t)}$ with slowly time-varying $a_k(t)$ and IF $\varphi_k'(t)$, where locally the component $x_k(t)$ can be regarded as a harmonic signal with amplitude $a_k(t)$ and IF $\varphi_k'(t)$ in the time domain. Both modeling harmonic-like signals, $\mathcal{A}_{\epsilon,d}$ is defined in the time domain but $\mathcal{H}_{\epsilon,d}$ is defined in the frequency domain.

Theorem 1 is the main result of the TEWT, which performs a theoretical analysis of TEWT for frequency-domain signals in the mathematical framework. Moreover, Theorem 1 uses an analytic wavelet $\psi(t)$, which can be constructed with a frequency modulation of a real and symmetric window $g(t)$ and is defined as [26]

$$
\psi(t) = g(t)e^{i\omega_\psi t} \tag{33}
$$

where ω_ψ is the center frequency of $\hat{\psi}(\omega)$, and it can be expressed as

$$
\hat{\psi}(\omega) = \int_R \psi(t)e^{-i\omega t}dt = \int_R g(t)e^{-i(\omega-\omega_\psi)t}dt = \hat{g}(\omega - \omega_\psi). \tag{34}
$$

If $g(t)$ is supported in $[-\Delta, \Delta]$, it means that $g(t) = 0$ for $|t| \ge \Delta$.

Theorem 1 *Let* $X(\omega) = \sum_{k=1}^{K} X_k(\omega) \in \mathcal{H}_{\epsilon,d}$, *and set* $\tilde{\epsilon} := \epsilon^{1/3}$. *Pick a wavelet* $\psi(t)$ *in Schwartz class such that* $g(t) = \psi(t)e^{-i\omega_\psi t}$ *is supported in* $[-\Delta, \Delta]$, *with* $\Delta < \frac{d}{2\omega_\psi}$.

Consider the WT $W_X^{\hat{\psi}}(b,a)$ of $X(\omega)$ with respect to $\hat{\psi}(\omega)$, and the TEWT $Te(b,a)$. Then, provided ϵ is sufficiently small, the following hold:

(a) $|W_X^{\hat{\psi}}(b,a)| > \tilde{\epsilon}$ only when, for some $k \in \{1,2,...,K\}$, $(b,a) \in T_k := \{(b,a); |\frac{\phi_k'(\frac{\omega_\psi}{a})-b}{a}| < \Delta\}$.

(b) For each $k \in \{1,\dots,K\}$, and $(b,a) \in T_k$ such that $|W_X^{\hat{\psi}}(b,a)| > \tilde{\epsilon}$, we have

$$|\hat{t}_X(b,a) - \phi_k'(\frac{\omega_\psi}{a})| \le \tilde{\epsilon}. \tag{35}$$

(c) Moreover, for each $k \in \{1,\dots,K\}$ such that,

$$|\frac{aTe(\phi_k'(\frac{\omega_\psi}{a}),a)e^{-i\frac{\omega_\psi}{a}\phi_k'(\frac{\omega_\psi}{a})}}{\psi^*(0)} - X_k(\frac{\omega_\psi}{a})| \le \frac{a\tilde{\epsilon}}{|\psi(0)|}. \tag{36}$$

The proof of Theorem 1 is divided into several simple estimates and lemma.

Estimate 1 For each $k \in \{1,\dots,K\}$, we have the following:

$$\begin{aligned} &|A_k(\omega) - A_k(\frac{\omega_\psi}{a})| \le \epsilon M_k'|\omega - \frac{\omega_\psi}{a}|, \\ &|\phi_k(\omega) - \phi_k(\frac{\omega_\psi}{a}) - \phi_k'(\frac{\omega_\psi}{a})(\omega - \frac{\omega_\psi}{a})| \le \frac{1}{2}\epsilon M_k'|\omega - \frac{\omega_\psi}{a}|^2. \end{aligned} \tag{37}$$

Proof When $\omega \ge \frac{\omega_\psi}{a}$, we have (the case $\omega < \frac{\omega_\psi}{a}$ can be done in an analogue way):

$$|A_k(\omega)-A_k(\frac{\omega_\psi}{a})| = |\int_{\frac{\omega_\psi}{a}}^{\omega} A_k'(x)dx| \le \int_{\frac{\omega_\psi}{a}}^{\omega} |A_k'(x)|dx \le \epsilon \int_{\frac{\omega_\psi}{a}}^{\omega} |\phi_k'(x)|dx \le \epsilon M_k'|\omega-\frac{\omega_\psi}{a}|, \tag{38}$$

On the other hand, it is easy to show that

$$\begin{aligned} &|\phi_k(\omega) - \phi_k(\frac{\omega_\psi}{a}) - \phi_k'(\frac{\omega_\psi}{a})(\omega - \frac{\omega_\psi}{a})| \\ &= |\int_{\frac{\omega_\psi}{a}}^{\omega} (\phi_k'(x) - \phi_k'(\frac{\omega_\psi}{a}))dx| = |\int_{\frac{\omega_\psi}{a}}^{\omega}\int_{\frac{\omega_\psi}{a}}^{x} \phi_k''(y)dydx| \\ &\le \int_{\frac{\omega_\psi}{a}}^{\omega}\int_{\frac{\omega_\psi}{a}}^{x} |\phi_k''(y)|dydx \le \epsilon M_k' \int_{\frac{\omega_\psi}{a}}^{\omega} |x - \frac{\omega_\psi}{a}|dx \\ &= \frac{1}{2}\epsilon M_k'|\omega - \frac{\omega_\psi}{a}|^2. \end{aligned} \tag{39}$$

To simplify the notation, in what follows, we set

$$\tilde{X}_k(\omega) = A_k(\frac{\omega_\psi}{a})e^{-i(\phi_k(\frac{\omega_\psi}{a})+\phi_k'(\frac{\omega_\psi}{a})(\omega-\frac{\omega_\psi}{a}))}. \tag{40}$$

Estimate 2 For each $k \in \{1,\dots,K\}$, and for $(b,a) \in R \times R^+$, we have:

$$\begin{aligned} &W_{\tilde{X}_k}^{\hat{\psi}}(b,a) = \frac{1}{a}X_k(\frac{\omega_\psi}{a})e^{i\frac{\omega_\psi}{a}b}g^*(\frac{\phi_k'(\frac{\omega_\psi}{a}) - b}{a}), \\ &W_{\tilde{X}_k}^{\hat{\psi}'}(b,a) = i(\frac{\phi_k'(\frac{\omega_\psi}{a}) - b}{a})W_{\tilde{X}_k}^{\hat{\psi}}(b,a), \end{aligned} \tag{41}$$

Furthermore, we have:

$$
\begin{aligned}
&|W_X^{\hat{\psi}}(b,a) - \sum_{k=1}^{K} W_{\tilde{X}_k}^{\hat{\psi}}(b,a)| \le \epsilon \mathit{\Omega}_1(a),\\
&|W_X^{\hat{\psi}'}(b,a) - \sum_{k=1}^{K} W_{\tilde{X}_k}^{\hat{\psi}'}(b,a)| \le \epsilon \mathit{\Omega}_2(a),
\end{aligned} \tag{42}
$$

where

$$
\begin{aligned}
\mathit{\Omega}_1(a) &= \sum_{k=1}^{K} (M_k' I_1(a) + \frac{1}{2} M_k M_k' I_2(a)),\\
\mathit{\Omega}_2(a) &= \sum_{k=1}^{K} (M_k' I_1'(a) + \frac{1}{2} M_k M_k' I_2'(a)).
\end{aligned} \tag{43}
$$

with

$$
\begin{aligned}
I_p(a) &= \frac{1}{2\pi} \int_R |\omega - \frac{\omega_\psi}{a}|^p |\hat{\psi}(a\omega)| d\omega,\\
I_p'(a) &= \frac{1}{2\pi} \int_R |\omega - \frac{\omega_\psi}{a}|^p |\hat{\psi}'(a\omega)| d\omega,\ p = 1, 2.
\end{aligned} \tag{44}
$$

Proof According to the WT definition (5), the WT $W_{\tilde{X}_k}^{\hat{\psi}}(b,a)$ of $\tilde{X}_k(\omega)$ with respect to wavelet $\hat{\psi}(\omega)$ can be calculated as

$$
\begin{aligned}
W_{\tilde{X}_k}^{\hat{\psi}}(b,a) &= \frac{1}{2\pi} \int_R \tilde{X}_k(\omega) \hat{\psi}^*(a\omega) e^{i\omega b} d\omega\\
&= \frac{1}{2\pi} A_k(\frac{\omega_\psi}{a}) e^{-i\phi_k(\frac{\omega_\psi}{a})} \int_R e^{-i\phi_k'(\frac{\omega_\psi}{a})(\omega - \frac{\omega_\psi}{a})} \hat{g}^*(a\omega - \omega_\psi) e^{i\omega b} d\omega\\
&= \frac{1}{2\pi a} X_k(\frac{\omega_\psi}{a}) e^{i\frac{\omega_\psi}{a} b} \int_R \hat{g}^*(\xi) e^{-i(\frac{\phi_k'(\frac{\omega_\psi}{a}) - b}{a})\xi} d\xi\\
&= \frac{1}{a} X_k(\frac{\omega_\psi}{a}) e^{i\frac{\omega_\psi}{a} b} g^*(\frac{\phi_k'(\frac{\omega_\psi}{a}) - b}{a}).
\end{aligned} \tag{45}
$$

where the third equality uses $\omega = \frac{\omega_\psi + \xi}{a}$. And $W_{\tilde{X}_k}^{\hat{\psi}'}(b,a)$ of $\tilde{X}_k(\omega)$ with respect to $\hat{\psi}'(\omega) = \hat{g}'(\omega - \omega_\psi)$ can be expressed as

$$
\begin{aligned}
W_{\tilde{X}_k}^{\hat{\psi}'}(b,a) &= \frac{1}{2\pi} \int_R \tilde{X}_k(\omega) \hat{\psi}'^*(a\omega) e^{i\omega b} d\omega\\
&= \frac{1}{2\pi} A_k(\frac{\omega_\psi}{a}) e^{-i\phi_k(\frac{\omega_\psi}{a})} \int_R e^{-i\phi_k'(\frac{\omega_\psi}{a})(\omega - \frac{\omega_\psi}{a})} \hat{g}'^*(a\omega - \omega_\psi) e^{i\omega b} d\omega\\
&= \frac{1}{2\pi a} X_k(\frac{\omega_\psi}{a}) e^{i\frac{\omega_\psi}{a} b} \int_R \hat{g}'^*(\xi) e^{-i(\frac{\phi_k'(\frac{\omega_\psi}{a}) - b}{a})\xi} d\xi\\
&= \frac{i}{a} X_k(\frac{\omega_\psi}{a}) e^{i\frac{\omega_\psi}{a} b} (\frac{\phi_k'(\frac{\omega_\psi}{a}) - b}{a}) g^*(\frac{\phi_k'(\frac{\omega_\psi}{a}) - b}{a})\\
&= i(\frac{\phi_k'(\frac{\omega_\psi}{a}) - b}{a}) W_{\tilde{X}_k}^{\hat{\psi}}(b,a).
\end{aligned} \tag{46}
$$

where $\hat{g}'(\omega) \leftrightarrow -itg(t)$.

On the other hand, for $(b,a)\in R\times R^+$, we have

$$
\begin{aligned}
&|W_X^{\hat\psi}(b,a)-\sum_{k=1}^K W_{\tilde X_k}^{\hat\psi}(b,a)\le\sum_{k=1}^K|W_{X_k}^{\hat\psi}(b,a)-W_{\tilde X_k}^{\hat\psi}(b,a)|\\
&\le\frac{1}{2\pi}\sum_{k=1}^K|\int_R(A_k(\omega)-A_k(\frac{\omega_\psi}{a}))e^{-i\phi_k(\omega)}\hat\psi^*(a\omega)e^{i\omega b}d\omega|\\
&+\frac{1}{2\pi}\sum_{k=1}^K|\int_R A_k(\frac{\omega_\psi}{a})(e^{-i\phi_k(\omega)}-e^{-i(\phi_k(\frac{\omega_\psi}{a})+\phi_k'(\frac{\omega_\psi}{a})(\omega-\frac{\omega_\psi}{a}))})\hat\psi^*(a\omega)e^{i\omega b}d\omega| \qquad (47)\\
&\le\frac{1}{2\pi}\sum_{k=1}^K\int_R|A_k(\omega)-A_k(\frac{\omega_\psi}{a})||\hat\psi(a\omega)|d\omega\\
&+\frac{1}{2\pi}\sum_{k=1}^K\int_R|A_k(\frac{\omega_\psi}{a})||\phi_k(\omega)-\phi_k(\frac{\omega_\psi}{a})-\phi_k'(\frac{\omega_\psi}{a})(\omega-\frac{\omega_\psi}{a})||\hat\psi(a\omega)|d\omega,
\end{aligned}
$$

where we use the differential mean value theorem $e^{ix}-e^{i0}=ie^{i\xi}x$, and according to Estimate 1, we have

$$
\begin{aligned}
&|W_X^{\hat\psi}(b,a)-\sum_{k=1}^K W_{\tilde X_k}^{\hat\psi}(b,a)|\\
&\le\sum_{k=1}^K\frac{\epsilon M_k'}{2\pi}(\int_R|\omega-\frac{\omega_\psi}{a}||\hat\psi(a\omega)|d\omega+\frac{1}{2}M_k\int_R|\omega-\frac{\omega_\psi}{a}|^2|\hat\psi(a\omega)|d\omega) \qquad (48)\\
&\le\epsilon\sum_{k=1}^K(M_k'I_1(a)+\frac{1}{2}M_kM_k'I_2(a))=\epsilon\Omega_1(a).
\end{aligned}
$$

and similarly,

$$
\begin{aligned}
&|W_X^{\hat\psi'}(b,a)-\sum_{k=1}^K W_{\tilde X_k}^{\hat\psi'}(b,a)|\le\sum_{k=1}^K|W_{X_k}^{\hat\psi'}(b,a)-W_{\tilde X_k}^{\hat\psi'}(b,a)|\\
&\le\frac{1}{2\pi}\sum_{k=1}^K|\int_R(A_k(\omega)-A_k(\frac{\omega_\psi}{a}))e^{-i\phi_k(\omega)}\hat\psi'^*(a\omega)e^{i\omega b}d\omega|\\
&+\frac{1}{2\pi}\sum_{k=1}^K|\int_R A_k(\frac{\omega_\psi}{a})(e^{-i\phi_k(\omega)}-e^{-i(\phi_k(\frac{\omega_\psi}{a})+\phi_k'(\frac{\omega_\psi}{a})(\omega-\frac{\omega_\psi}{a}))})\hat\psi'^*(a\omega)e^{i\omega b}d\omega|\\
&\le\frac{1}{2\pi}\sum_{k=1}^K\int_R|A_k(\omega)-A_k(\frac{\omega_\psi}{a})||\hat\psi'(a\omega)|d\omega \qquad (49)\\
&+\frac{1}{2\pi}\sum_{k=1}^K\int_R|A_k(\frac{\omega_\psi}{a})||\phi_k(\omega)-\phi_k(\frac{\omega_\psi}{a})-\phi_k'(\frac{\omega_\psi}{a})(\omega-\frac{\omega_\psi}{a})||\hat\psi'(a\omega)|d\omega\\
&\le\sum_{k=1}^K\frac{\epsilon M_k'}{2\pi}(\int_R|\omega-\frac{\omega_\psi}{a}||\hat\psi'(a\omega)|d\omega+\frac{1}{2}M_k\int_R|\omega-\frac{\omega_\psi}{a}|^2|\hat\psi'(a\omega)|d\omega)\\
&\le\epsilon\sum_{k=1}^K(M_k'I_1'(a)+\frac{1}{2}M_kM_k'I_2'(a))=\epsilon\Omega_2(a).
\end{aligned}
$$

The following lemma indicates that each zone T_k does not intersect with each other:

Lemma 1 For $k \in \{1, \ldots, K-1\}$, $T_{k+1} \bigcap T_k = \emptyset$ when $d > 2\omega_\psi \Delta$.

Proof If $(b, a) \in T_k$, then we have

$$\phi_k'(\frac{\omega_\psi}{a}) - a\Delta < b < \phi_k'(\frac{\omega_\psi}{a}) + a\Delta. \tag{50}$$

According to separation condition (32) and $d > 2\omega_\psi \Delta$, we have $\phi_{k+1}'(\frac{\omega_\psi}{a}) - \phi_k'(\frac{\omega_\psi}{a}) \geq \frac{ad}{\omega_\psi} > 2a\Delta$, which is equivalent to $\phi_{k+1}'(\frac{\omega_\psi}{a}) - a\Delta > \phi_k'(\frac{\omega_\psi}{a}) + a\Delta$. It means that the lower boundary of the zones T_{k+1} is above the upper boundary of the zones T_k, i.e. $T_{k+1} \bigcap T_k = \emptyset$.

Proof of Theorem 1 (a) If $(b, a) \notin T_k$, i.e. $|\frac{\phi_k'(\frac{\omega_\psi}{a}) - b}{a}| \geq \Delta$, then $g(\frac{\phi_k'(\frac{\omega_\psi}{a}) - b}{a}) = 0$. Thus, when $(b, a) \notin \bigcup_{1 \leq k \leq K} T_k$, by (41), we have

$$\sum_{k=1}^{K} W_{\tilde{X}_k}^{\hat{\psi}}(b, a) = \frac{1}{a} \sum_{k=1}^{K} X_k(\frac{\omega_\psi}{a}) e^{i\frac{\omega_\psi}{a} b} g^*(\frac{\phi_k'(\frac{\omega_\psi}{a}) - b}{a}) = 0. \tag{51}$$

By (42), it follows that $|W_X^{\hat{\psi}}(b, a)| \leq \epsilon \Omega_1(a)$. According to Lemma 1, assume ϵ satisfies

$$\epsilon^{\frac{2}{3}} \Omega_1(a) \leq 1, \tag{52}$$

then $|W_X^{\hat{\psi}}(b, a)| > \tilde{\epsilon}$ only when, for some $k \in \{1, 2, ..., K\}$, $(b, a) \in T_k$.

Estimate 3 For $k \in \{1, \ldots, K\}$, and $(b, a) \in T_k$, we have:

$$\begin{aligned} &|W_X^{\hat{\psi}}(b, a) - W_{\tilde{X}_k}^{\hat{\psi}}(b, a)| \leq \epsilon \Omega_1(a), \\ &|W_X^{\hat{\psi}'}(b, a) - W_{\tilde{X}_k}^{\hat{\psi}'}(b, a)| \leq \epsilon \Omega_2(a). \end{aligned} \tag{53}$$

Proof For $(b, a) \in T_k (k \neq \ell)$, i.e. $(b, a) \notin T_\ell$, $|\frac{\phi_\ell'(\frac{\omega_\psi}{a}) - b}{a}| \geq \Delta$, then $g(\frac{\phi_\ell'(\frac{\omega_\psi}{a}) - b}{a}) = 0$ and by (41), we have

$$\sum_{1 \leq \ell \neq k \leq K}^{K} W_{\tilde{X}_\ell}^{\hat{\psi}}(b, a) = 0. \tag{54}$$

Thus, we have

$$\begin{aligned} |W_X^{\hat{\psi}}(b, a) - W_{\tilde{X}_k}^{\hat{\psi}}(b, a)| &\leq |W_X^{\hat{\psi}}(b, a) - \sum_{k=1}^{K} W_{\tilde{X}_k}^{\hat{\psi}}(b, a)| + |\sum_{1 \leq \ell \neq k \leq K}^{K} W_{\tilde{X}_\ell}^{\hat{\psi}}(b, a)| \\ &\leq \epsilon \Omega_1(a). \end{aligned} \tag{55}$$

Moreover, for $(b,a) \in T_k (k \neq \ell)$, i.e. $(b,a) \notin T_\ell$, assume $|\frac{\phi'_\ell(\frac{\omega_\psi}{a})-b}{a}| < \infty$, and by (41), we have

$$\sum_{1\leq \ell \neq k \leq K}^{K} W_{\tilde{X}_\ell}^{\hat{\psi}'}(b,a) = i \sum_{1\leq \ell \neq k \leq K}^{K} (\frac{\phi'_\ell(\frac{\omega_\psi}{a}) - b}{a}) W_{\tilde{X}_\ell}^{\hat{\psi}}(b,a) = 0. \tag{56}$$

Thus, we have

$$\begin{aligned} |W_X^{\hat{\psi}'}(b,a) - W_{\tilde{X}_k}^{\hat{\psi}'}(b,a)| &\leq |W_X^{\hat{\psi}'}(b,a) - \sum_{k=1}^{K} W_{\tilde{X}_k}^{\hat{\psi}'}(b,a)| + |\sum_{1\leq \ell\neq k\leq K}^{K} W_{\tilde{X}_\ell}^{\hat{\psi}'}(b,a)| \\ &\leq \epsilon \Omega_2(a). \end{aligned} \tag{57}$$

Next, we will consider the error analysis of the GD estimator and the true GD.

Estimate 4 Suppose that (52) is satisfied. For $k \in \{1, \ldots, K\}$, and $(b,a) \in T_k$ such that $|W_X^{\hat{\psi}}(b,a)| > \tilde{\epsilon}$, then we have

$$|\tilde{t}_X(b,a) - \phi'_k(\frac{\omega_\psi}{a})| \leq \epsilon^{\frac{2}{3}} \Gamma(a), \tag{58}$$

where $\Gamma(a) = a(\Omega_2(a) + \Omega_1(a)\Delta)$.

Proof By definition, $\tilde{t}_x(b,a)$ is the complex reassignment operator of $\hat{t}_x(b,a)$, and expressed as

$$\tilde{t}_X(b,a) = b - ia \frac{W_X^{\hat{\psi}'}(b,a)}{W_X^{\hat{\psi}}(b,a)} \tag{59}$$

we have then

$$\begin{aligned} |\tilde{t}_X(b,a) - \phi'_k(\frac{\omega_\psi}{a})| &= |b - ia \frac{W_X^{\hat{\psi}'}(b,a)}{W_X^{\hat{\psi}}(b,a)} - \phi'_k(\frac{\omega_\psi}{a})| \\ &= |a \frac{W_X^{\hat{\psi}'}(b,a)}{W_X^{\hat{\psi}}(b,a)} + i(b - \phi'_k(\frac{\omega_\psi}{a}))| \\ &= |a \frac{W_X^{\hat{\psi}'}(b,a) - i\frac{(\phi'_k(\frac{\omega_\psi}{a})-b)}{a} W_X^{\hat{\psi}}(b,a)}{W_X^{\hat{\psi}}(b,a)}| \\ &\leq |a \frac{W_X^{\hat{\psi}'}(b,a) - i\frac{(\phi'_k(\frac{\omega_\psi}{a})-b)}{a} W_{\tilde{X}_k}^{\hat{\psi}}(b,a)}{W_X^{\hat{\psi}}(b,a)}| \\ &+ |a \frac{\frac{\phi'_k(\frac{\omega_\psi}{a})-b}{a}(W_X^{\hat{\psi}}(b,a) - W_{\tilde{X}_k}^{\hat{\psi}}(b,a))}{W_X^{\hat{\psi}}(b,a)}|, \end{aligned} \tag{60}$$

According to Estimate 2, for $(b,a) \in T_k$, i.e. $|\frac{\phi'_k(\frac{\omega_\psi}{a})-b}{a}| \leq \Delta$, so that

$$
\begin{aligned}
|\tilde{t}_X(b,a)-\phi_k'(\frac{\omega_\psi}{a})| &\le |a\frac{W_X^{\hat{\psi}'}(b,a)-W_{\tilde{X}_k}^{\hat{\psi}'}(b,a)}{W_X^{\hat{\psi}}(b,a)}|+|a\frac{\frac{\phi_k'(\frac{\omega_\psi}{a})-b}{a}(W_X^{\hat{\psi}}(b,a)-W_{\tilde{X}_k}^{\hat{\psi}}(b,a))}{W_X^{\hat{\psi}}(b,a)}| \\
&\le \epsilon^{\frac{2}{3}}a(\Omega_2(a)+\Omega_1(a)\Delta)=\epsilon^{\frac{2}{3}}\Gamma(a).
\end{aligned}
\tag{61}
$$

Proof of Theorem 1 (b) By (8), $\hat{t}_x(b,a)=\Re\{\tilde{t}_x(b,a)\}$, then

$$
\begin{aligned}
|\hat{t}_X(b,a)-\phi_k'(\frac{\omega_\psi}{a})| &= |\Re\{\tilde{t}_X(b,a)\}-\phi_k'(\frac{\omega_\psi}{a})| \\
&\le |\tilde{t}_X(b,a)-\phi_k'(\frac{\omega_\psi}{a})| \le \epsilon^{\frac{2}{3}}\Gamma(a),
\end{aligned}
\tag{62}
$$

If we impose an extra restriction on ϵ as follows

$$
\epsilon^{\frac{1}{3}}\Gamma(a)<1,
\tag{63}
$$

the estimate can be simplified to

$$
|\hat{t}_X(b,a)-\phi_k'(\frac{\omega_\psi}{a})| \le \tilde{\epsilon}.
\tag{64}
$$

Finally, we will consider the error of component recovered by TEWT.

Proof of Theorem 1 (c) Since $\psi^*(t)=g^*(t)e^{-i\omega_\psi t}$, $\psi^*(0)=g^*(0)$, we evaluate the WT in (41) along the ridge line $b=\phi_k'(\frac{\omega_\psi}{a})$ of $X_k(\omega)$ leading to

$$
\begin{aligned}
W_{\tilde{X}_k}^{\hat{\psi}}(\phi_k'(\frac{\omega_\psi}{a}),a) &= \frac{1}{a}X_k(\frac{\omega_\psi}{a})e^{i\frac{\omega_\psi}{a}\phi_k'(\frac{\omega_\psi}{a})}g^*(0) \\
&= \frac{1}{a}X_k(\frac{\omega_\psi}{a})e^{i\frac{\omega_\psi}{a}\phi_k'(\frac{\omega_\psi}{a})}\psi^*(0),
\end{aligned}
\tag{65}
$$

thus,

$$
X_k(\frac{\omega_\psi}{a})=\frac{aW_{\tilde{X}_k}^{\hat{\psi}}(\phi_k'(\frac{\omega_\psi}{a}),a)e^{-i\frac{\omega_\psi}{a}\phi_k'(\frac{\omega_\psi}{a})}}{\psi^*(0)}.
\tag{66}
$$

According to Estimate 3, and when ϵ satisfies (52) and (63), we have

$$
\begin{aligned}
&|\frac{aTe(\phi_k'(\frac{\omega_\psi}{a}),a)e^{-i\frac{\omega_\psi}{a}\phi_k'(\frac{\omega_\psi}{a})}}{\psi^*(0)}-X_k(\frac{\omega_\psi}{a})| \\
&\le |\frac{a}{\psi^*(0)}|W_X^{\hat{\psi}}(\phi_k'(\frac{\omega_\psi}{a}),a)-W_{\tilde{X}_k}^{\hat{\psi}}(\phi_k'(\frac{\omega_\psi}{a}),a)|| \\
&+|\frac{aW_{\tilde{X}_k}^{\hat{\psi}}(\phi_k'(\frac{\omega_\psi}{a}),a)e^{-i\frac{\omega_\psi}{a}\phi_k'(\frac{\omega_\psi}{a})}}{\psi^*(0)}-X_k(\frac{\omega_\psi}{a})| \\
&\le \epsilon|\frac{a}{\psi(0)}|\Omega_1(a)\le\frac{a\tilde{\epsilon}}{|\psi(0)|}
\end{aligned}
\tag{67}
$$

The proof of Theorem 1 is finished.

5 Numerical experiments

To explore the performance of the TEWT comprehensively, we employ the third-order Rényi entropy [3, 4] and the reconstruction quality factor (RQF) [11, 12] to quantify the analysis results. The RQF is defined as

$$RQF = 10 \log_{10} \frac{\|x(t)\|^2}{\|x(t) - x_r(t)\|^2}. \tag{68}$$

where $x(t)$ and $x_r(t)$ denote the noise-free signal and the reconstructed signal, respectively. Generally, a higher RQF value means better reconstruction performance. Besides, we compare TEWT and four TFA medthos, including WT, SWT, MSWT and TSST. For the analysis function used in the numerical experiments, WT, SWT, MSWT and TEWT use Morlet wavelet, TSST uses the Gaussian window function.

5.1 Frequency-domain signal

The test signal $X(\omega)$ contains two components ($X_1(\omega)$ and $X_2(\omega)$) and is defined in the frequency domain:

$$X(\omega) = X_1(\omega) + X_2(\omega) = A_1(\omega)e^{-i\phi_1(\omega)} + A_2(\omega)e^{-i\phi_2(\omega)}, \tag{69}$$

where

$$\begin{cases} A_1(\omega) = A_2(\omega) = e^{0.001\omega}, \\ \phi_1(\omega) = -0.001\omega^3 + 0.16\omega^2 + 1.2\omega, \\ \phi_2(\omega) = 0.03\omega^2 + 5.2\omega + 250 \ln(0.05\omega + 0.6). \end{cases} \tag{70}$$

This signal is sampled at 512 points and its sampling frequency is 128 Hz.

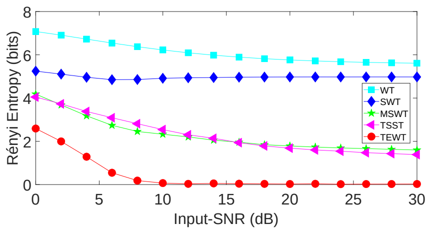

Fig. 2: Under different noise levels, Rényi entropy curves of TFRs generated by different TFA methods.

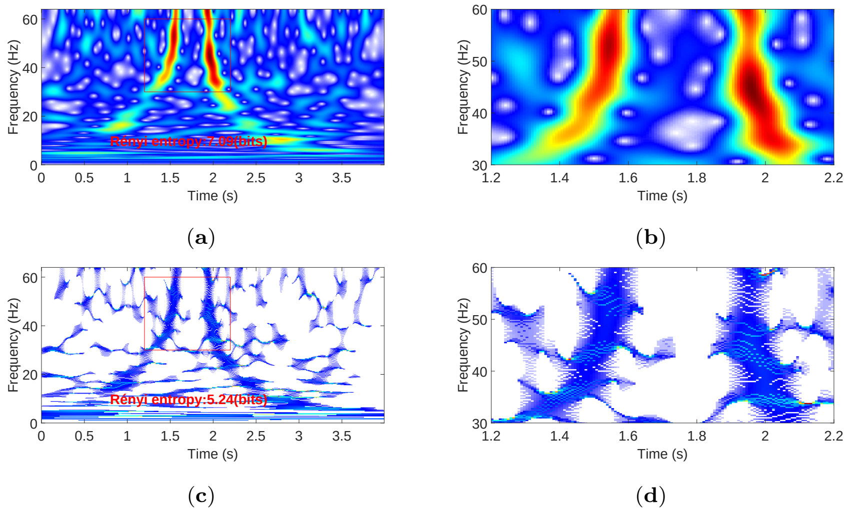

Fig. 3: The comparison study of the test signal with zero dB Gaussian white noise: (a) WT, (b) zoom of the WT, (c) SWT, (d) zoom of the SWT.

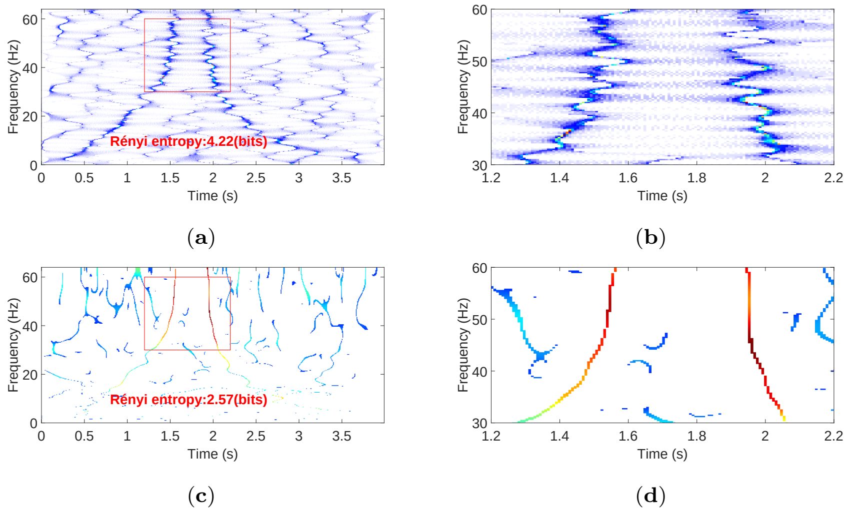

Fig. 4: The comparison study of the test signal with zero dB Gaussian white noise: (a) TSST, (b) zoom of the TSST, (c) TEWT, (d) zoom of the TEWT.

Fig. 2 shows the third-order Rényi entropy curves of five TFA methods (WT, SWT, MSWT, TSST and TEWT) for frequency-domain signal $X(\omega)$ with different noise levels, where $X(\omega)$ is added with Gaussian white noises ranging from 0 to 30 dB of SNR, and the Rényi entropy will decrease with the improvement of the energy concentration of TFR. It can be seen that under any noise level, WT has the

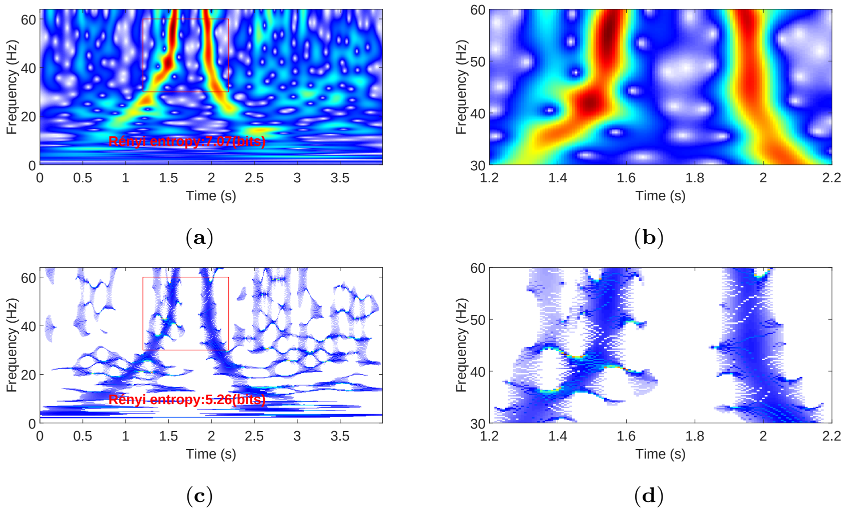

Fig. 5: The comparison study of the test signal with SNR=0 dB impulsive noise: (a) WT, (b) zoom of the WT, (c) SWT, (d) zoom of the SWT.

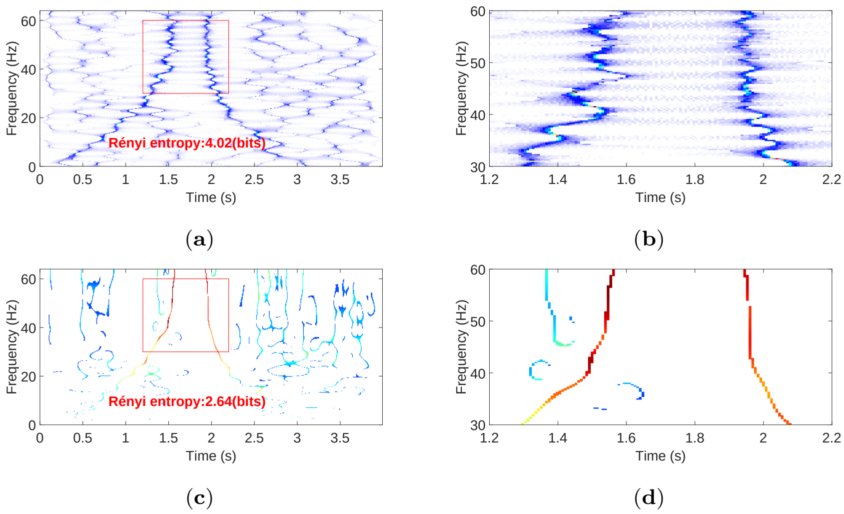

Fig. 6: The comparison study of the test signal with SNR=0 dB impulsive noise: (a) TSST result, (b) zoom of the TSST, (c) TEWT, (d) zoom of the TEWT.

largest Rényi entropy value, which means WT obtains the worst TF concentration performance. As post-processing methods of WT, SWT, MSWT and TEWT all have much smaller Rényi entropy values than WT, thus these post-processing methods have greatly improved the TF concentration performance of the WT. Compared with the other four TFA methods, TEWT has the smallest Rényi entropies at each noise level, which indicates that the TEWT performs the best ability to improve the TF energy concentration and achieves the best TFR result among all the methods. This can be specifically illustrated by Figs. 3-6.

In Figs. 3-4, we added Gaussian white noise with SNR=0 dB to the signal to verify the TF performance of TEWT in the noise situations, and we compare the TFR results generated by WT, SWT, TSST, TEWT and their zoomed-versions, where the third-order Rényi entropies are showed in each picture. It can be observed that WT, SWT and TSST suffer diffuse TFRs and are very sensitive to noise. Compared to these TFA methods, the proposed TEWT in Fig. 4 (c), (d) obtains the lowest Rényi entropy value, reaches the best TFR result while improving the noise robustness. Moreover, we added impulsive noise with SNR=0 dB to the signal in Figs. 5-6, which further verify the superiority of TF performance of TEWT in the noise situations. Thus, Figs. 2-6 clearly demonstrate that the TEWT is superior to other methods in terms of TF energy concentration and noise robustness performance.

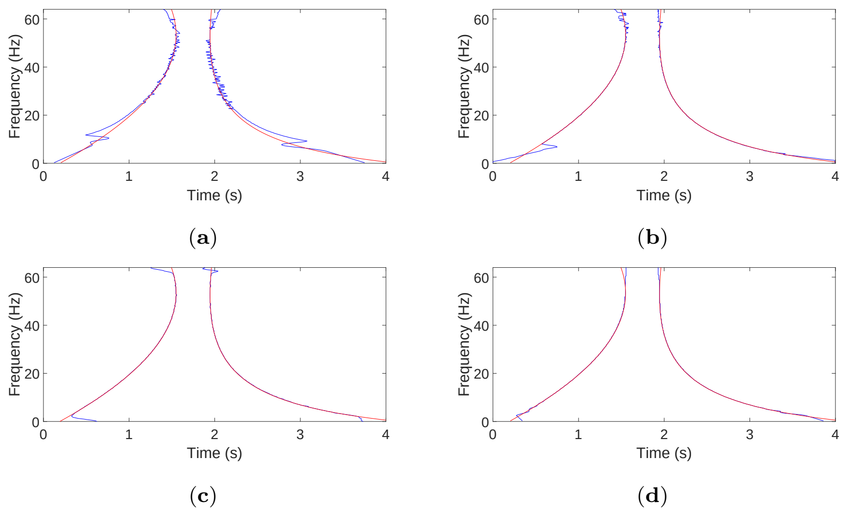

Fig. 7: The comparisons of GD estimation: (a) SWT, (b) MSWT, (c) TSST, (d) TEWT.

Furthermore, we compare the GD estimation of four TFA methods for $X(\omega)$ under noise-free situation in Fig. 7, red lines denotes true GD trajectories, blue lines denote estimated GD trajectories. It can be found that SWT in Fig. 7 (a), designed for slowly varying signals (satisfying $|\varphi_k''(t)| \to 0$), fails to estimate the GD of $X(\omega)$ whose TF

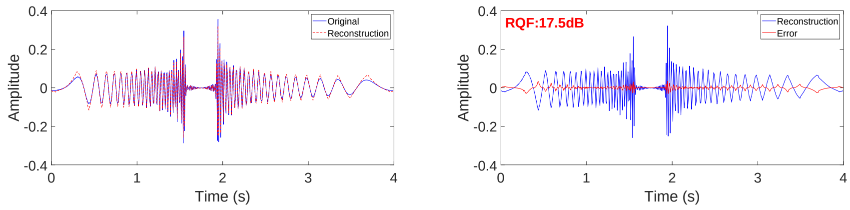

Fig. 8: (a) The original signal and the reconstructed signal, (b) The reconstructed signal and the reconstructed error.

ridge curves that changes rapidly or even perpendicular to the time axis. For the MSWT that is suitable for fast-varying signals (satisfying $|\varphi_k''(t)| < \infty$) in Fig. 7 (b), it greatly improves the GD estimation accuracy of SWT. However, TSST and TEWT, designed for impulsive-like signal (satisfying $|\varphi_k''(t)| \to \infty$) whose TF ridge curves nearly perpendicular to the time axis, provide more precise GD estimations. By carefully comparing (c) and (d) in Fig. 7, TEWT provides a slightly better GD estimation than TSST, thus TEWT provides a more accurate GD estimation for frequency domain signals than other TFAs.

Finally, the second quantified indicator RQF is used to evaluate the reconstruction performance of TEWT in Fig. 8, which is written in the picture. Fig. 8 (a) compares the original signal (blue line) and the signal reconstructed (red line) by TEWT, and Fig. 8 (b) compares the reconstructed signal (blue line) and reconstructed error (red line) by TEWT. The reconstructed signal, reconstructed error and the RQF (17.5 dB) in Fig. 8 all verify that TEWT can reconstruct the signal very accurately and has good reconstruction performance. Therefore, for frequency domain signals, TEWT performs well in terms of TF energy concentration, noise robustness, GD estimation and reconstruction performance.

5.2 Time-domain numerical fault signal

A numerical fault signal with a rapidly changing status is modeled according to the mechanical theory [36], the analysis results generated by the TEWT and classical TFA methods and their zoomed-versions are shown in Fig. 9 and Fig. 10. The sampling frequency is 1024 Hz, and time duration is [0, 1].

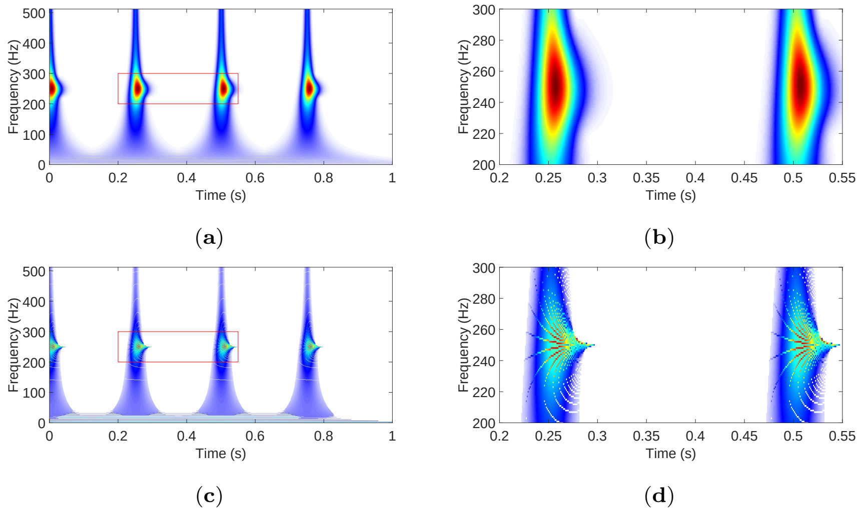

Fig. 9: (a) WT result, (b) zoom of the WT result, (c) SWT result, (d) zoom of the SWT result.

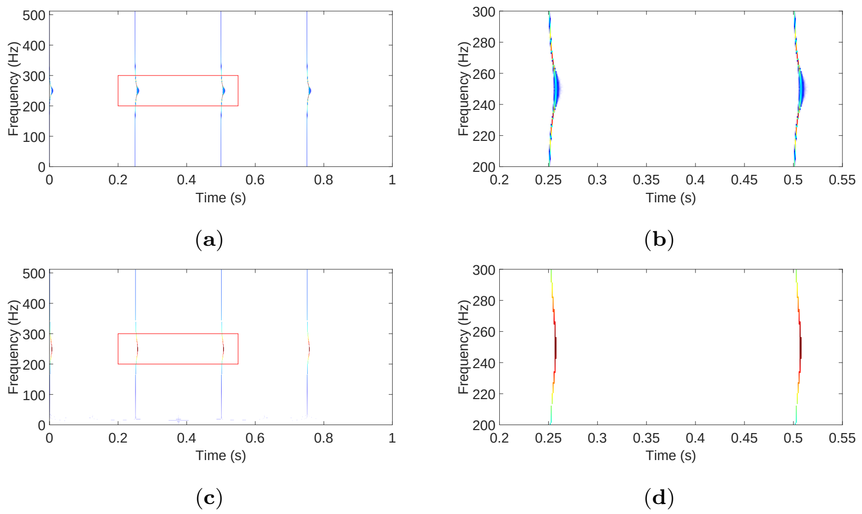

Fig. 10: (a) TSST result, (b) zoom of the TSST result, (c) TEWT result, (d) zoom of the TEWT result.

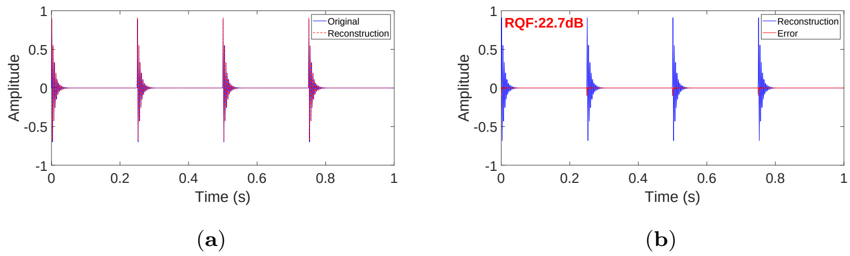

Fig. 11: (a) The original signal and the reconstructed signal, (b) The reconstructed signal and the reconstructed error.

It can be seen that in Fig. 9, restricted to the Heisenberg uncertainty principle, WT in Fig. 9 (a) provide a blurry TF explanation for the time-domain fault signal. Since SWT adopts the time-domain harmonic-like signal model and squeezes the WT coefficients along the frequency direction, which makes SWT unable to provide an energy-concentrated TFR for the fault signal in Fig. 9 (c). Compared with WT and SWT in Fig. 9, it can be observed that TSST greatly improves the TF resolution of fault signal in Fig. 10 (a), but TEWT provides a higher-resolution TFR in Fig. 10 (c) and obtains the most concentrated TFR among all the methods, thus TEWT is more suitable to characterize the TF feature of fault signal. Next, we verify the reconstruction performance of TEWT in Fig. 11. As shown in Fig. 11 (a), the signal reconstructed by TEWT is highly consistent with the time-domain fault signal, and the reconstruction error and RQF (22.7 dB) in Fig. 11 (b) also further verify the accuracy of TEWT reconstruction. It can be concluded that the TEWT behaves the best TF performance and perfect reconstruction performance.

5.3 Bat signal

A bat signal recorded is employed to validate the effectiveness of the TEWT [39], which is sampled at 400 points and its sampling frequency is 140 kHz. The waveform of the signal and its spectrum are displayed in Fig. 12 (a), (b), it can be observed that it is far from enough to describe the features of the signal only from its waveform and spectrum, so the TFA method is needed to further characterize the signal. In order to characterize the bat signal precisely, we used four TFA methods

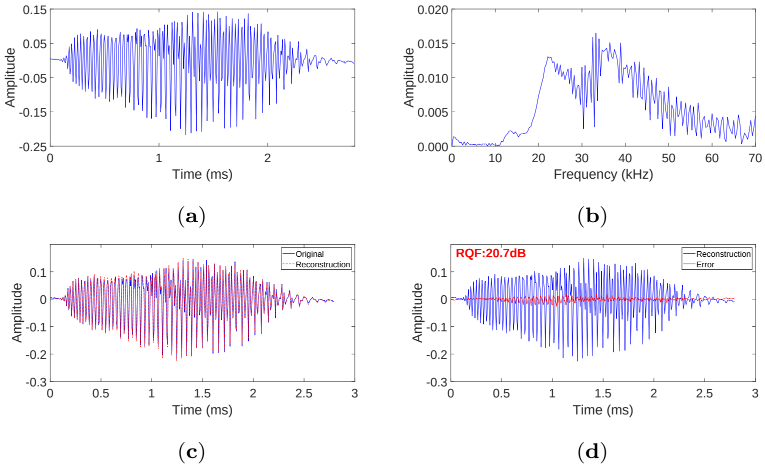

Fig. 12: (a) The waveform of the bat signal, (b) The spectrum of the bat signal, (c) The original signal and the reconstructed signal, (d) The reconstructed signal and the reconstructed error.

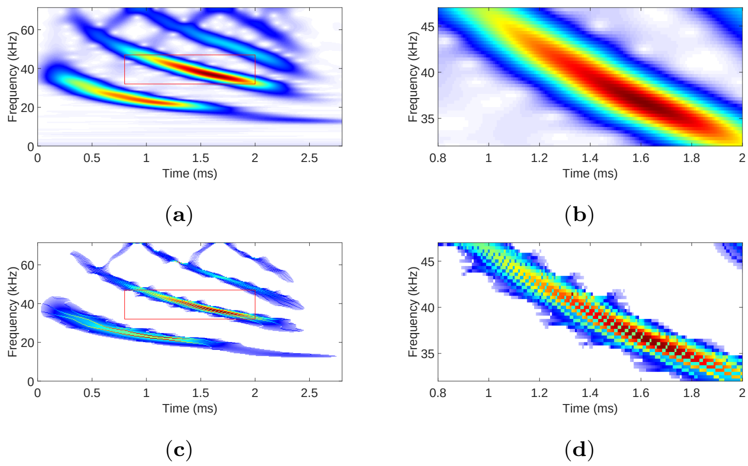

Fig. 13: (a) WT result, (b) zoom of the WT result, (c) SWT result, (d) zoom of the SWT result.

to process the bat signal in Figs. 13, 14, including WT, SWT, TSST and TEWT. The analysis results show that the TEWT has the best performance to generate the most energy-concentrated TFR among above TFA methods. Fig. 12 (c), (d) shows the reconstructed results by TEWT, it can be seen that TEWT can reconstruct signals extremely well and obtain a high RQF (20.7 dB), thus TEWT has the good reconstruction ability. Therefore, the TEWT is suitable for characterizing the bat signal.

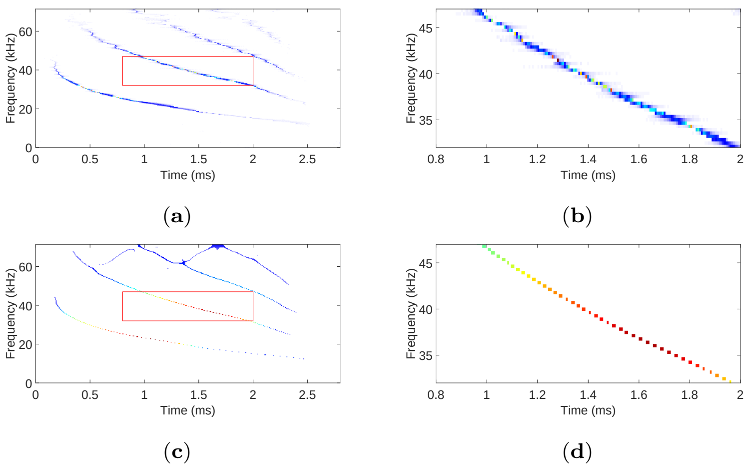

Fig. 14: (a) TSST result, (b) zoom of the TSST result, (c) TEWT result, (d) zoom of the TEWT result.

6 Conclusion

The two contributions of this paper are the proposal of TEWT and the theoretical analysis of TEWT for frequency-domain signals. In this regard, for the impulsive signal and its frequency-domain harmonic signal, we propose the TEWT that achieves highly-concentrated TFRs while allowing signal reconstruction, only by retaining the closely-related TF energy with discarding weakly-related TF information. On the other hand, we provide a rigorous theoretical analysis of TEWT under a mathematical framework for the frequency-domain signal model. Specifically, we define a function class as a set of all superposition of well-separated frequency-domain harmonic-like functions, where each function can be locally regarded as a sum of a finite number of harmonic signals in the frequency domain, and establish error bounds for WT approximate expression, GD estimation and component recovery. Finally, we verify the superiority of the TEWT in terms of the concentration, robustness, and invertibility with two quantitative indicators, by using numerical experiments of frequency-domain signals, time-domain signals and real signals. It can be concluded that theoretical analysis and numerical experiments demonstrate that TEWT is a powerful tool for analyzing time-domain impulsive-like signals or frequency-domain harmonic-like signals.

Acknowledgements This work was supported by National Natural Science Foundation of China under Grant U20B2075, the ANR ASCETE project with grant number ANR-19-CE48-0001-01 and the Fundamental Research Funds for the Central Universities under Grant G2021KY05103. The authors thank the editor and the anonymous reviewers for their valuable comments and suggestions that helped improve the quality of this paper.

Data availability statement The datasets analyzed during the current study are available from the corresponding author on reasonable request.

Declarations

Conflict of interest The authors declare that they have no conflict of interest.

References

1. F. Auger, P. Flandrin, Improving the readability of time-frequency and time-scale representations by the reassignment method. IEEE Trans. Signal Process. **43**(5), 1068-1089 (1995)
2. F. Auger, P. Flandrin, Y. Lin, S. McLaughlin, S. Meignen, T. Oberlin, H.T. Wu, Time-frequency reassignment and synchrosqueezing: an overview. IEEE Signal Process. Mag. **30**(6), 32-41 (2013)
3. S. Aviyente, W.J. Williams, Minimum entropy time-frequency distributions, IEEE Signal Process. Lett. **12**(1), 37-40 (2005)
4. R.G. Baraniuk, P. Flandrin, A.J.E.M. Janssen, O.J.J. Michel, Measuring time-frequency information content using the Rényi entropies. IEEE Trans. Inf. Theory. **47**, 1391-1409, (2001)
5. R. Behera, S. Meignen, T. Oberlin, Theoretical analysis of the second order synchrosqueezing transform. Appl. Comput. Harmon. Anal. **45**(2), 379-404 (2018)
6. E. Chassande-Mottin, F. Auger, P. Flandrin, Time frequency/time scale reassignment, in Wavelets and signal processing. 233-268 (2003).
7. L. Cohen, *Time-Frequency Analysis* (Prentice-Hall, Englewood Cliffs, NJ, 1995)
8. I. Daubechies, J.F. Lu, H.T. Wu, Synchrosqueezed wavelet transforms: an empirical mode decomposition-like tool. Appl. Computat. Harmon. Anal. **30**, 243-261 (2011)
9. I. Daubechies, S. Maes, A nonlinear squeezing of the continuous wavelet transform. Wavelets in Medecine and Bio. 527-546 (1996)
10. P. Flandrin, F. Auger, E. Chassande-Mottin, Time-frequency reassignment: from principles to algorithms, in Applications in Time-Frequency Signal Processing (CRC, Arizona), 179-203 (2003)
11. D. Fourer, F. Auger, P. Flandrin, Recursive versions of the Levenberg-Marquardt reassigned spectrogram and of the synchrosqueezed STFT. in Proc. IEEE ICASSP. 4880-4884 (2016)
12. D. Fourer, F. Auger, K. Czarnecki, S. Meignen, and P. Flandrin, Chirp rate and instantaneous frequency estimation: application to recursive vertical synchrosqueezing, IEEE Signal Process. Lett. **24**(11), 1724-1728 (2017)

13. B. Han, Y. Zhou, G. Yu, Second-order synchroextracting wavelet transform for nonstationary signal analysis of rotating machinery, Signal Process. **186**, 108123 (2021)
14. D. He, H. Cao, S. Wang, X. Chen, Time-reassigned synchrosqueezing transform: The algorithm and its applications in mechanical signal processing, Mech. Syst. Signal Process. **117**, 255-279 (2019)
15. Y. Hu, X. Tu, F. Li, High-order synchrosqueezing wavelet transform and application to planetary gearbox fault diagnosis. Mech. Syst. Signal Process. **131**, 126-151 (2019)
16. N.E. Huang, Z. Shen, S.R. Long, M.L. Wu, H.H. Shih, Q. Zheng, N.C. Yen, C.C. Tung, H.H. Liu, The empirical mode decomposition and Hilbert spectrum for nonlinear and non-stationary time series analysis. Proc. Roy. Soc. London A, **454**, 903-995 (1998).
17. Z. Huang, J. Zhang, Z. Zou, Synchrosqueezing s-transform and its application in seismic spectral decomposition. IEEE Trans. Geosci. Remote Sens. **54** (2), 817-825 (2016)
18. K. Kodera, R. Gendrin, and C. de Villedary, Analysis of time-varying signals with small BT values. IEEE Trans. Acoust. Speech. Signal Process. ASSP, **26**(1), 64-76 (1978)
19. K. Kodera, C. de Villedary, and R. Gendrin, A new method for the numerical analysis of non-stationary signals. Phys. Earth. Plan. Int. **12**, 142-150 (1976)
20. C. Li, M. Liang, A generalized synchrosqueezing transform for enhancing signal time-frequency representation. Signal Process. **92**(9), 2264-2274 (2012)
21. W. Li, F. Auger, Z. Zhang, X. Zhu, Self-matched extracting wavelet transform and signal reconstruction. Digital Signal Processing. **128**, 103602 (2022)
22. W. Li, Z. Zhang, F. Auger, X. Zhu, Theoretical analysis of time-reassigned synchrosqueezing wavelet transform[J]. Applied mathematics letters. **132**, 108141 (2022)
23. Z. Li, J. Gao, H. Li, et al, Synchroextracting transform: The theory analysis and comparisons with the synchrosqueezing transform. Signal Process. **166**, 107243 (2020)
24. J.M. Lilly, S.C. Olhede, On the analytic wavelet transform. IEEE Trans. Inform. Theor. **56**(8), 4135-4156 (2010)
25. N. Liu, J. Gao, X. Jiang, Z. Zhang, Q. Wang, Seismic time-frequency analysis via STFT-based concentration of frequency and time. IEEE Geosci. Remote. Sens. Lett. **14**(1), 127-131 (2017)
26. S. Mallat, *A Wavelet Tour of Signal Processing: The Sparse Way (3rd edn)* (Academic Press, Burlington, 2009)
27. Z. H. Michalopoulou, Underwater transient signal processing: Marine mammal identification, localization, and source signal deconvolution. ICASSP, IEEE International Conference on Acoustics, Speech and Signal Processing-Proceedings. **1**, 503-506 (1997)
28. Z. K. Peng, G. Meng, F. L. Chu, Z. Q. Lang, W. M. Zhang, Y. Yang, Polynomial chirplet transform with application to instantaneous frequency estimation. IEEE Trans. Instrum. Meas. **60**(9), 3222-3229 (2011)
29. D.H. Pham, S. Meignen, High-order synchrosqueezing transform for multicomponent signals analysis-with an application to gravitational-wave signal. IEEE Trans. Signal Process. **65**(12), 3168-3178 (2017)

30. J. Pons-Llinares, J.A. Antonino-Daviu, M. Riera-Guasp, S. Bin Lee, T.J. Kang, C. Yang, Advanced induction motor rotor fault diagnosis via continuous and discrete time-frequency tools. IEEE Trans. Indust. Electron. **62**(3), 1791-1802 (2015)
31. J. Shi, M. Liang, D.S. Necsulescu, Y. Guan, Generalized stepwise demodulation transform and synchrosqueezing for time-frequency analysis and bearing fault diagnosis. J. Sound Vib. **368**, 202-222 (2016)
32. G. Thakur, H.T. Wu, Synchrosqueezing-based recovery of instantaneous frequency from nonuniform samples, SIAM J. Math. Anal. **43** (5), 2078C2095 (2011)
33. X. Tu, Y. Hu, F. Li, S. Abbas, Z. Liu, W. Bao, Demodulated high-order synchrosqueezing transform with application to machine fault diagnosis. IEEE Trans. Ind. Electron. **66**(4), 3071-3081 (2018)
34. S. Wang, X. Chen, G. Cai, B. Chen, X. Li, Z. He, Matching demodulation transform and synchrosqueezing in time-frequency analysis. IEEE Trans. Signal Process. **62** (1), 69-84 (2014)
35. S. Wang, X. Chen, I.W. Selesnick, Y. Guo, C. Tong, X. Zhang, Matching synchrosqueezing transform: a useful tool for characterizing signals with fast varying instantaneous frequency and application to machine fault diagnosis. Mech. Syst. Signal Process. **100**, 242-288 (2018)
36. G. Yu, A concentrated time-frequency analysis tool for bearing fault diagnosis. IEEE Trans. Instrum. Meas. **69**(2), 371-381 (2019)
37. K. Yu, H. Ma, H. Han, Second order multi-synchrosqueezing transform for rub-impact detection of rotor systems. Mech. Mach. Theory. **140**, 321-349 (2019)
38. G. Yu, Z. Wang, P. Zhao, Multi-synchrosqueezing transform. IEEE Trans. Ind. Electron. **66**(7), 5441-5455 (2019)
39. G. Yu, M. Yu, C. Xu, Synchroextracting transform. IEEE Trans. Ind. Electron. **64**(10), 8042-8054 (2017)
40. X. Zhu, Z. Zhang, J. Gao, Three-dimension extracting transform. Signal Process. **179**, 107830 (2021)
41. X. Zhu, Z. Zhang, J. Gao, B. Li, Z. Li, X. Huang, G. Wen, Synchroextracting chirplet transform for accurate IF estimate and perfect signal reconstruction. Dig. Signal Process. **93**, 172-186 (2019)
42. X. Zhu, Z. Zhang, Z. Li, J. Gao, X. Huang, G. Wen, Multiple squeezes from adaptive chirplet transform. Signal Process. **163**, 26-40 (2019)